Available online at www.sciencedirect.com
ScienceDirect
Journal of Power Sources 167 (2007) 111–117
JOURNAL OF POWER SOURCES
www.elsevier.com/locate/jpowsour

Intermediate temperature solid oxide fuel cell based on $BaIn_{0.3}Ti_{0.7}O_{2.85}$ electrolyte

D. Prakash [1], T. Delahaye, O. Joubert, M.-T. Caldes, Y. Piffard *

CNRS, Université de Nantes, Nantes Atlantique Universités, Institut des Matériaux Jean ROUXEL, UMR no. 6502, 2, rue de la Houssinière, BP 32229-44322 Nantes Cedex 3, France

Received 20 November 2006; received in revised form 19 January 2007; accepted 5 February 2007
Available online 17 February 2007

Abstract

Electrolyte supported as well as anode supported single-cells based on $BaIn_{0.3}Ti_{0.7}O_{2.85}$ (BIT) electrolyte were developed. In these cells, Ni-BIT cermet was used as anode and $La_{0.8}Sr_{0.2}MnO_3$ as cathode. Electrolyte supported cells were fabricated by coating slurries of anode and cathode materials on the circular faces of sintered electrolyte discs. The maximum power (P_{max}) drawn was 15 mW cm^{-2} at 30 mA cm^{-2}. Anode supported cells were fabricated by co-pressing and co-sintering anode and electrolyte powders. The thickness of electrolyte in anode supported cells was reduced to 80 μm and the area specific resistance decreased considerably. The value of P_{max} improved to ∼100 mW cm^{-2}.

Keywords: SOFC; Electrolyte; Barium indium titanate

1. Introduction

Solid oxide fuel cells (SOFC) are considered as one of the most important futuristic electricity generation technologies using renewable resources [1,2]. Besides being highly efficient in terms of chemical to electrical energy ratio, this mode of energy conversion establishes its merit in terms of fuel-flexibility and environment-friendliness [3,4]. The SOFC derives its name due to the presence of an oxygen ion conducting electrolyte, separating oxidizing and reducing (fuel-rich) atmospheres. Due to chemical potential gradient, transport of oxygen ions across the electrolyte takes place resulting in electrochemical potential as can be described by the Nernst equation. The most commonly used electrolyte material in SOFC is yttria stabilized zirconia (YSZ), exhibiting sufficient values of ionic conductivities (>10^{-2} S cm^{-1}) above 1000 °C, thus making practically operable fuel cell systems at such high temperatures. This high operational temperature poses various problems such as restricted choice of sealing and interconnect materials, degradation reactions, insulation and stability of the system. Therefore, it has been continuous endeavor of researchers to bring down the operating temperature of SOFC in the range 750–800 °C, either by reducing the YSZ electrolyte thickness or by finding alternative electrolytes. Colloïdal fabrication and co-sintering processes have emerged, whereby YSZ membranes are deposited as thin layers (∼10 μm) on porous electrode materials and in the meantime a variety of materials such as doped Ceria, $LaGaO_3$, $La_2Mo_2O_9$, $Ba_2In_2O_5$, etc. have been discovered as potential electrolyte materials [5].

In previous studies, it has been shown that substitution of In by Ti in brownmillerite compound $Ba_2In_2O_5$ induces disorder in the ordered arrangement of oxygen vacancies [6]. At higher substitution levels (>15%), the compound converts into a disordered cubic perovskite structure at room temperature, exhibiting better anionic conductivity than the parent $Ba_2In_2O_5$ phase [6,7]. The disordered perovskite compound $BaIn_{0.3}Ti_{0.7}O_{2.85}$ (BIT) is oxygen ion conductor with a conductivity similar to that of YSZ. This makes BIT as potential candidate for electrolyte material at intermediate temperatures.

It is well known that in a SOFC system, the choice of a new electrolyte material calls for suitable selection of anode and cathode materials also. In a recent study, suitability of

* Corresponding author. Tel.: +33 2 40 37 39 13; fax: +33 2 40 37 39 95.
E-mail addresses: deep_prakash@rediffmail.com (D. Prakash), Thibaud.Delahaye@cnrs-imn.fr (T. Delahaye), Olivier.Joubert@cnrs-imn.fr (O. Joubert), Maite.Caldes@cnrs-imn.fr (M.-T. Caldes), Yves.Piffard@cnrs-imn.fr (Y. Piffard).
[1] Permanent address: Energy Conversion Materials Section, Bhabha Atomic Research Centre, Vashi Complex, Navi Mumbai 400705, India.

0378-7753/$ – see front matter © 2007 Elsevier B.V. All rights reserved.
doi:10.1016/j.jpowsour.2007.02.014

Ni-BIT as anode material has already been established [8]. The present study shows the development of single-cells based on BIT electrolyte. The paper describes fabrication of electrolyte supported as well as anode supported single-cells. Microstructural features of the cells were examined and their performances were evaluated under different fuels.

2. Experimental work

Two different configurations of cells, based on BIT electrolyte were investigated in this study, the electrolyte supported (type-E) and the anode supported (type-A). The preparation and characterization of these cells are described below.

2.1. Synthesis of materials

The BIT powder used in this study was prepared by conventional solid state mixing and grinding route. The constituents, high purity barium carbonate and indium oxide (Alfa Aesar, Germany) and titanium dioxide (Rhône Poulenc) were weighed as per the stoichiometric ratio and mixed in mortar and pestle using alcohol. The mixture was first calcined at 1200 °C for 24 h, then ground and compacted into a pellet of 40 mm diameter. This compact was then heated at 1350 °C for 24 h, ground and passed through mesh 100. Prior to its use for preparation of anode composite pellets, the purity of this powder was checked by X-ray diffraction. A detailed report on the anode composite was published earlier [8]. The composite powder for anode substrates was prepared by mixing NiO and BIT powders in weight ratio of 30:70 on a roller bank. A part of the BIT powders was also ball-milled for 24 h in a FRITSCH planetary mill (Pulverisette 7) using alcohol. The ball-milled BIT powder was used for electrolyte layer. High purity $La_{0.8}Sr_{0.2}MnO_3$ (LSM) (Praxair Inc.) was used as cathode throughout the experiments.

2.2. Preparation of single-cells

As mentioned earlier, two different types of cells were used in this study. Fig. 1(a and b) shows flow-sheets of preparation of the cells. The electrolyte supported cell consisted of a dense pellet of BIT, coated on one side with anode and the other side with cathode materials. The BIT pellet was obtained by making compacts of ball-milled BIT powders in a 13 mm diameter die at a pressure of 40 MPa, followed by sintering at 1350 °C for 2 days. Anode, as well as cathode were formed by depositing organic slurries on the two circular faces of the pellet, respectively. Composition of the slurry is given in Table 1. These slurries were prepared separately, by mixing components in a ball-mill using a two-stage ball-milling procedure [9]. The anode slurry coated pellets were heat-treated at 1200 °C for 12 h, subsequent to which cathode slurry was applied on the other side of pellets, and the samples were heat-treated at 1000 °C for 12 h.

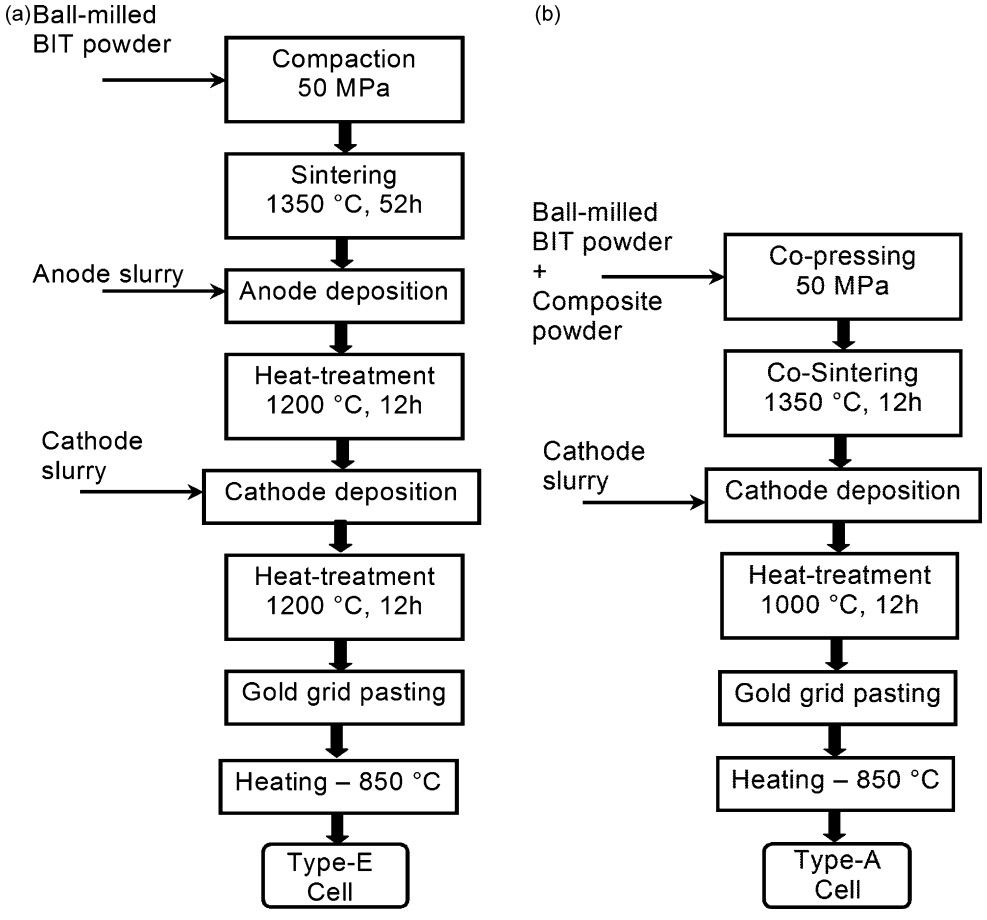

Fig. 1. Flow-sheets for preparation of (a) type-E cells and (b) type-A cells.

Table 1
Composition of the slurry for anode in type-E cell and cathode in type-E and type-A cells

Component	Quantity
Powder (NiO-BIT for anode and LSM for cathode)	10 g
Oleic acid	0.5 cm^3
Ethanol	5 cm^3
Methyl ethyl ketone	5 cm^3
Poly ethylene glycol	0.75 cm^3
Di octyl phthalate	0.60 cm^3
Poly vinyl butyral	0.5 g

To prepare anode supported (type-A) cells, the composite and ball-milled BIT powders were charged in 10 mm diameter die sequentially and pressed at a pressure of 50 MPa. In order to maintain interconnected porosity within the sintered sample to facilitate gas diffusion, 5 wt% sugar powder was added to the composite as pore former. The co-pressed pellets were sintered at 1350 °C for 12 h, resulting in an anode supported configuration. Formation of cathode layer was done by slurry coating on the electrolyte layer, followed by sintering, as done in the case of type-E cells.

For both the cell types mentioned above, the methodology adapted for converting the layered samples into single-cells was similar. In order to efficiently collect current from the surface of the cells, gold grid (wire thickness 60 μm, grid opening 250 μm) was cut into 6 mm circular discs, sewed with 50 μm thick gold wires and pasted on both the electrodes using gold ink. The cells were then heated at 850 °C for 20 min to evaporate the organics and to obtain good electrical and physical contacts.

2.3. Testing of single-cell

The single-cells were tested in a laboratory-made system for measurement of current–voltage (*I–V*) characteristics. Fig. 2 shows a schematic diagram of the system. The system contains an alumina sample tube (O.D. 10 mm, I.D. 6 mm), above which the button cells were pasted using Aremco sealing material (#503), thus separating the atmospheres between the inside and outside of tube. A fuel-gas supply tube (O.D, 4 mm, I.D. 2 mm) that is situated inside the sample tube, extends up to 10 mm off the anode surface. This tube is used for supply of fuel gas in the vicinity of the sample, and also houses the gold wire for electrical contact to the inside of the sample. Another gold contact wire is placed in the sample tube, outside the fuel-gas supply tube. Both the gold wires were connected to the inside of the sample. Outside of the sample tube, another tube with two small holes carries two platinum wires to the top surface of the sample. All the four wires were taken out separately from the system and connected to the electrical measuring equipment for characterization of the cell. The button cells were baked as per the instructions provided by sealant manufacturer prior to beginning of the measurements.

The system was kept vertically in a tubular furnace with flowing air as well as fuel-gas atmospheres maintained at the either surfaces of the cells.

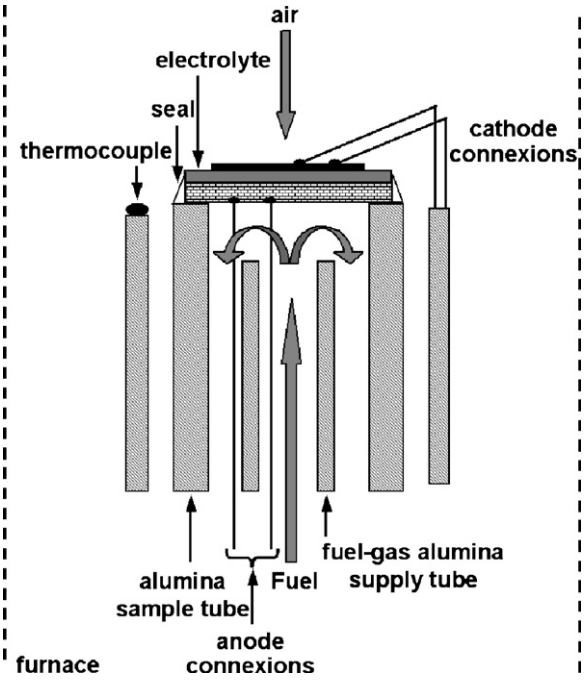

Fig. 2. Schematic diagram of the cell-testing apparatus.

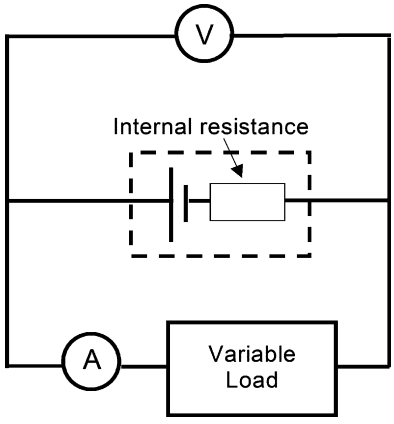

Fig. 3. Circuit diagram for the characterization of single-cells.

The measurements of current and voltage were done by digital multimeters Keithley 197 and Protek 506, respectively, as per the schematic diagram shown in Fig. 3. Current drawn in the circuit was varied using the rheostat. Effective area of the cells used in this study was 0.25 cm^2.

Microstructural features of the samples were examined by Scanning Electron Microscopy using JEOL JSM 5800 LV.

3. Results and discussion

Fig. 4(a–c) shows SEM photomicrographs of transverse sections of a electrolyte supported cell. It is noticed from Fig. 4(a) that the average thickness of the electrolyte layer is approximately 550 μm, whereas thicknesses of the anode as well as cathode layers are less than 100 μm. The electrolyte is fairly dense and well sintered with negligible porosity, whereas microstructures of anode as well as cathode exhibit

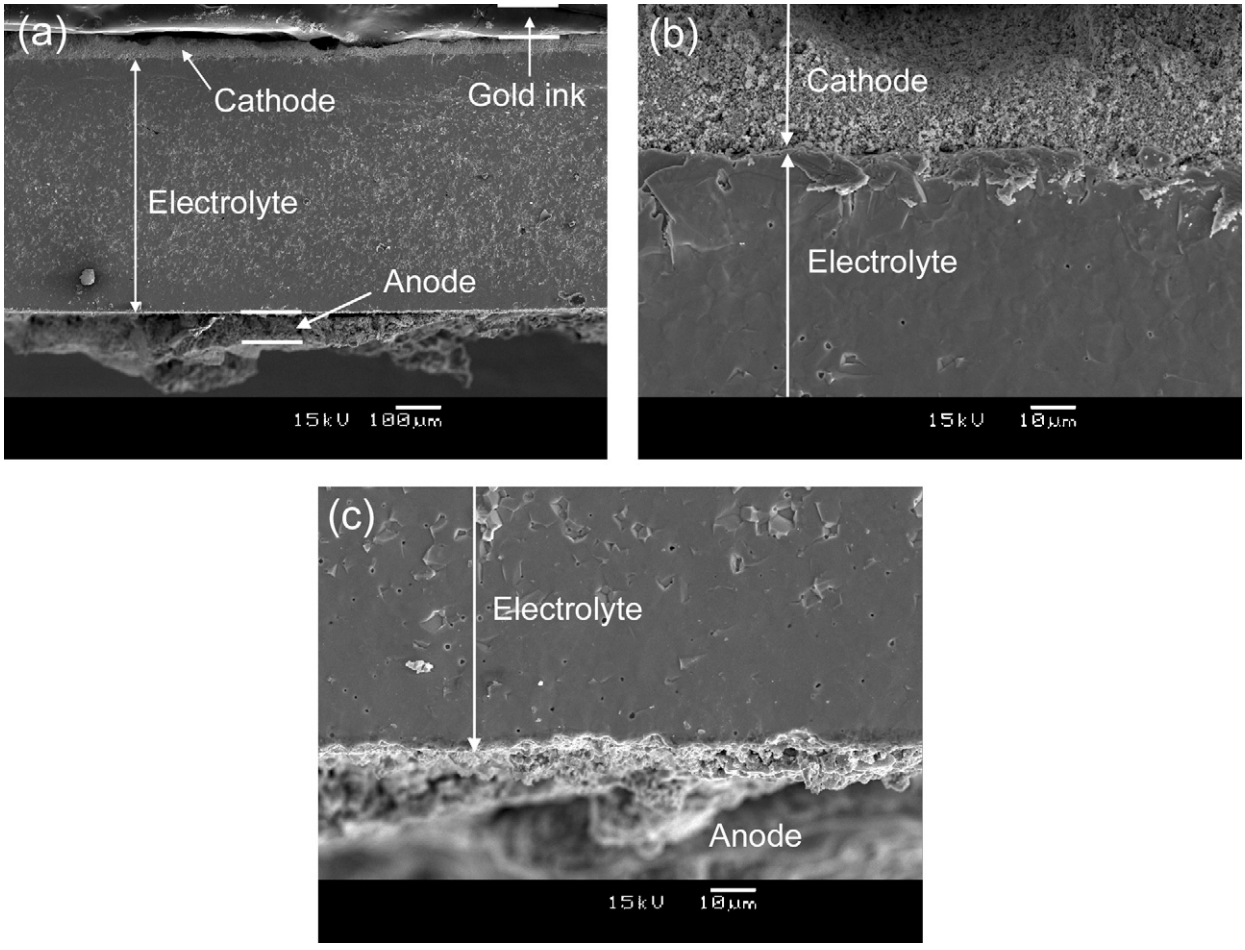

Fig. 4. SEM micrographs of an electrolyte supported cell showing: (a) anode, electrolyte and cathode layers, (b) cathode–electrolyte interface, and (c) electrolyte–anode interface.

interconnected porosity. This combination of controlled porosities in the SOFC components is a characteristic feature controlling high open circuit voltages, which depends on dense electrolyte (nil porosity), and higher performance depending on open pores with large triple-phase boundary areas.

I–V curves of the electrolyte supported (type-E) cell are shown in Fig. 5(a and b). Fig. 5(a) shows the measurements recorded in flowing hydrogen gas under dry and wet conditions ($p_{H_2O} = 0.025$ atm) at 810 °C. Under dry H_2 atmosphere, the open circuit voltage (OCV) was 1.046 V, indicating good sealing and nil leakage in the sample cell. The cell was equilibrated at high temperature to study the effect of time on the *I–V* characteristics. During the measurements there was no significant change in the OCV, however, slope of the curve improved marginally with time. This may be attributed to the gradual reduction of the NiO in the anode thus decreasing its ohmic resistance, as well as increasing number of triple-phase boundaries. The improvement in resistance was accompanied with shifting of the power maxima (P_{max}) slightly higher (13 mW cm^{-2}) after 18 h as compared to 10 mW cm^{-2} at only 20 min after the beginning of the reduction process. Beyond this time, no further decrease of the slope was observed, indicating completion of the reduction process.

Under wet hydrogen, the OCV decreased to 0.976 V due to a higher p_{O_2} than when dry hydrogen is used; however the slope of the *I–V* curve decreased indicating improvement in the overall performance of the cell. The slope under wet hydrogen was found to be as 20.3 Ω cm^2 as against 23.4 Ω cm^2 under dry hydrogen. The slope in the *I–V* plot represents a combination of ohmic resistances present in the cell and electrode over-potentials. It is well known that over-potential of Ni-YSZ anode decreases sharply with the presence of moisture in the atmosphere [10]. This is due to the fact that the electrochemical anode reaction is a complex process involving activation and diffusion of hydrogen, oxygen and steam. The presence of steam is likely to accelerate the electrochemical reaction and thereby decreasing the over-potential [11]. Since in the anode cermet, Ni-particles are responsible for anodic reaction, it can be surmised that similar phenomenon may be responsible for decrease of over-potential in Ni-BIT anode in the present study.

The *I–V* curve of type-E cell under dry natural gas (NG) fuel at 690 °C is shown in Fig. 5(b). The *I–V* plot under wet H_2 is also shown for comparative purpose. Under NG, the cell exhibited lower values of current densities. The *I–V* plot also shows a sharp decrease in the slope beyond 0.4 mA cm^{-2}. This feature is characteristic of concentration polarization. Cracking of natural gas may lead to carbon deposition in the anode, giving rise to depressed anodic reaction, and the present electrical data strongly suggest coking. However, on visual examination of the

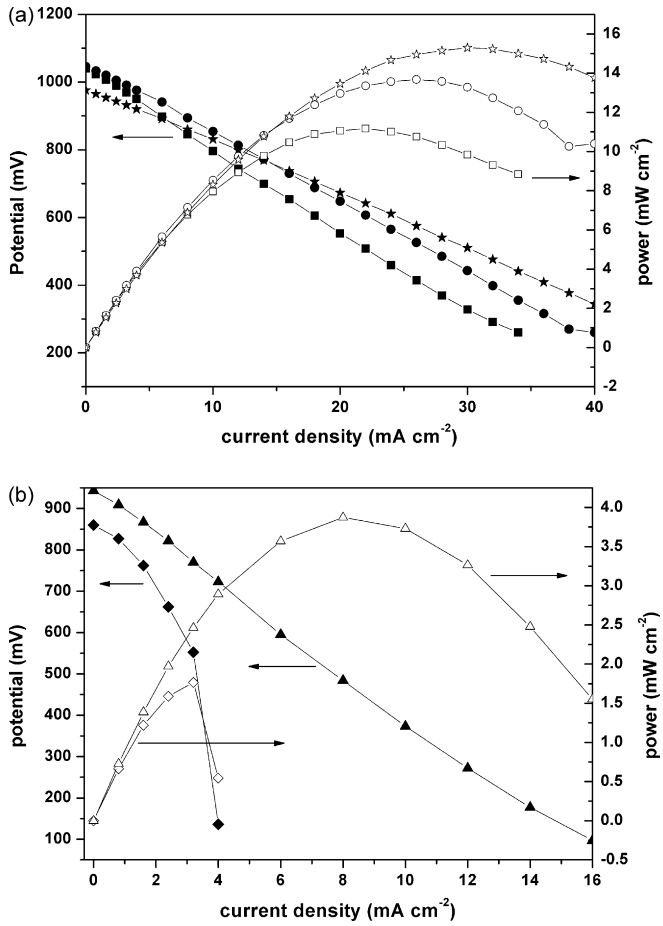

Fig. 5. *I–V* and power density curves of a single type-E cell: (a) anode under dry H_2 at 810 °C (after 20 min: squares; after 18 h: circles) and wet H_2 (after 20 h: stars) and cathode under air; (b) anode under natural gas (lozenges) and hydrogen (triangles) at 690 °C.

cell at the end of measurements there was no significant change in color of the anode surface, but it must be mentioned that the experiment under NG lasted for about 30 min only.

Fig. 6(a–c) shows *I–V* curves of anode supported bi-layer cell (type-A). Under the wet Ar–5% H_2 at 810 °C, the OCV was greater than 0.9 V, and the max power density was 52 mW cm^{-2} (Fig. 6(a)). Changing the atmosphere to pure wet hydrogen, increased the maximum current density more than 200 mA cm^{-2} (Fig. 6(b)). It can be noticed from the curve that the maxima of the power curve has not been attained. Considering that the polarization curve is a straight line where the slope is the total internal resistance (R_{int}), an estimate of the maximum power drawn in the fuel cell can be made using equation $P_{max} = V_0^2/(4R_{int})$ (Appendix A). By this method, in type-A cell, the maximum power was estimated as 90 mW cm^{-2}. It may be noted here that the open circuit voltage of the cell is only 0.9 V, thus indicating possibility of small leakage in either of the gas chambers. If it is assumed that this lowering of OCV is only due to leakage then the power maxima can be estimated to be more than 100 mW cm^{-2}.

The cell characteristics under NG and dry hydrogen at 690 °C are shown in Fig. 6(c). The value of P_{max} under hydrogen was found to be 14 mW cm^{-2} whereas that under NG was

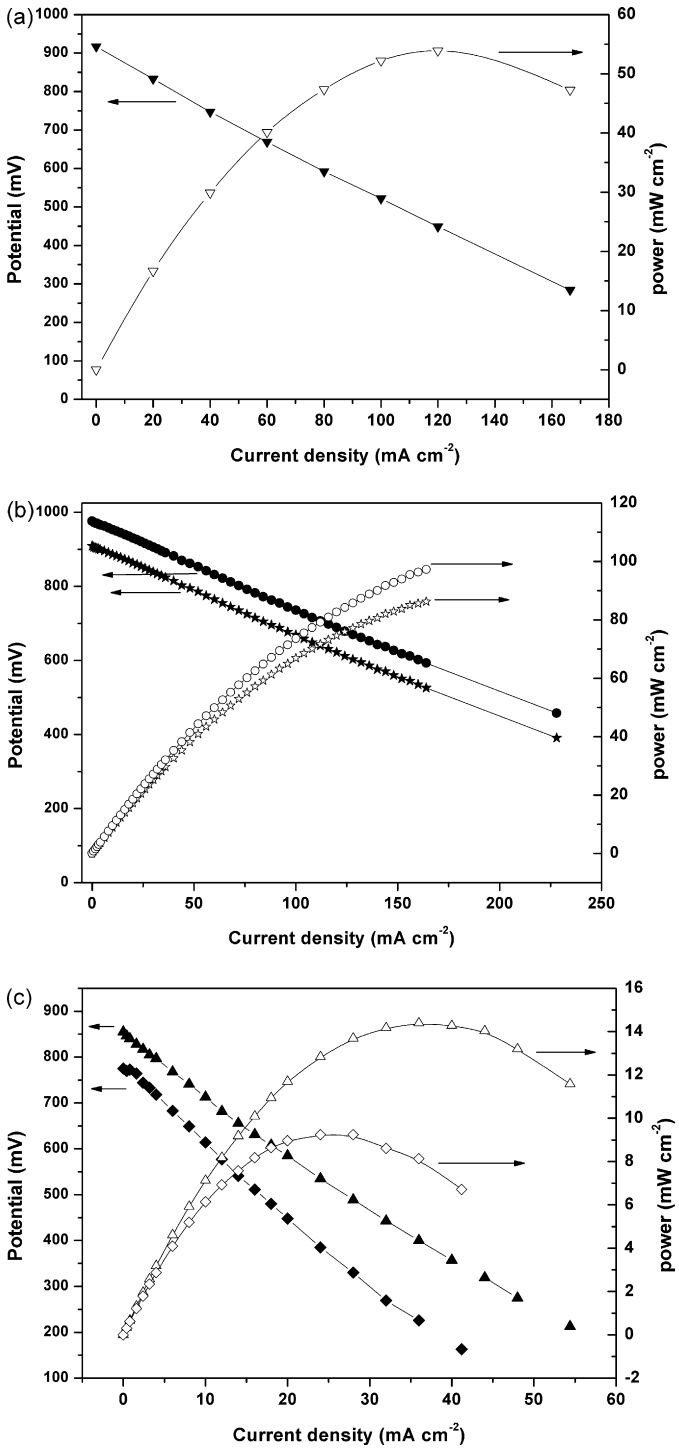

Fig. 6. *I–V* and power density curves of single type-A cell: (a) anode under wet Ar–5% H_2 at 810 °C, (b) anode under wet H_2 (as measured: stars; assuming no leak: circles) at 810 °C, and (c) anode under natural gas (lozenges) and hydrogen (triangles) at 690 °C.

8 mW cm^{-2}. These values are much higher than corresponding values obtained for type-E cell (3.7 and 1.5 mW cm^{-2}, respectively). The *I–V* plots are also linear and no effect of concentration polarization is apparent as found in the case of type-E cell, although the experiment lasted for 4 h. This suggests a better stability under NG than in the case of type-E cells.

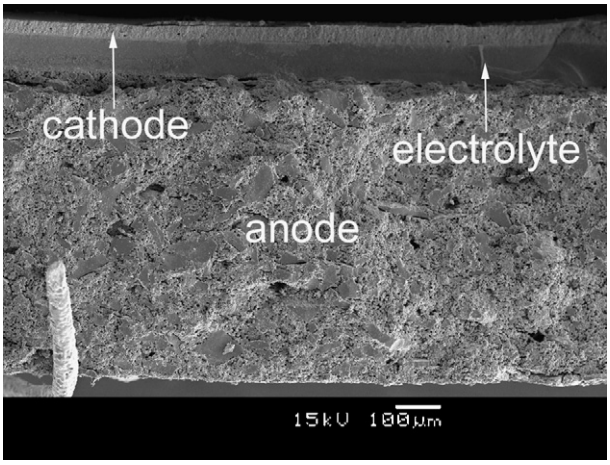

Fig. 7. SEM micrograph of a type-A cell.

In general, the values of power densities achieved in type-A cells are much higher than those observed in type-E cells. This is due to the fact that the thickness of electrolyte layer in type-A cells is much less than that in type-E cells. Since at these temperatures, ohmic resistance of the electrolyte layer is the most significant contributor to the internal resistance of the cell, reducing the electrolyte layer results in improving the current density.

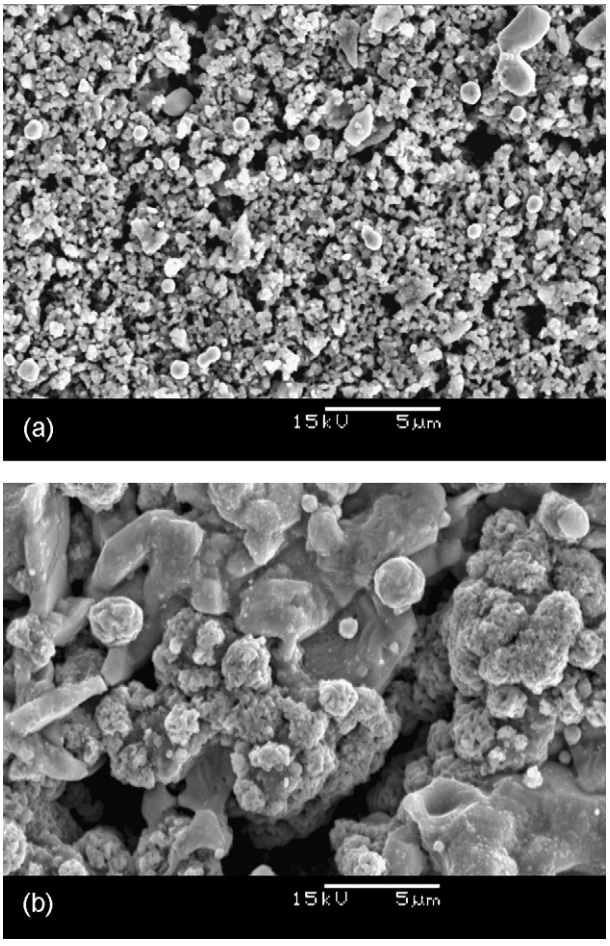

Fig. 8. Microstructure of the anode in (a) type-E cell and (b) type-A cell.

Fig. 7 shows SEM micrographs taken from section of type-A cell. The thickness of electrolyte layer is approximately 80 μm. A lowered thickness of electrolyte layer is perhaps the main reason behind a reduced value of internal resistance, measured as 2.3 Ω cm^2 from *I–V* plot (Fig. 6(b)). Comparing this value of R_{int} with that of type-E cell, it follows that the value of R_{int} is not in direct proportion to decrease in layer thickness. This can be ascribed to the fact that the slope of *I–V* curve includes electrode over-potential besides the ohmic resistances. Anodes of both the cells differ largely in fabrication processing that can bear significant influence on the microstructures and hence anodic over-potentials. Fig. 8(a and b) shows the anode microstructures in type-E and type-A cells, respectively. Though the total volumetric content of porosities is comparable, a clear difference in pore structure is noticed. Pore structure in anode of type-E cell is finer but nickel particles in type-A anode are much porous. This may result in a combination of more triple-phase boundary area and better connectivity between Ni-particles, thus contributing to the lowered values of internal resistances in type-A anode, that is to a better electro-catalytic behavior.

4. Conclusions

This study shows that $BaIn_{0.3}Ti_{0.7}O_{2.85}$ is a potential electrolyte material for SOFC applications at intermediate temperatures. Two types of single-cells, electrolyte supported as well as anode supported were fabricated and tested. It follows that thickness of the electrolyte is one of the major factor contributing to the internal resistance of the cells. Cells with lower electrolyte thickness indicate stability under natural gas, which is useful for natural gas utilization.

Acknowledgements

Authors are thankful to Alain Barreau for his help in SEM experiments. One of the authors (DP) acknowledges support of Région des Pays de La Loire for post doctoral fellowship.

Appendix A

Assuming linear nature of potential with current density,

$$V = V_0 - jR_{int} \quad (A.1)$$

where V is potential, V_0 the OCV, j the current density and R_{int} is slope of the *I–V* curve. Therefore,

$$P = jV = j(V_0 - jR_{int}) \quad (A.2)$$

for maximum power differentiating P and equating dP/dj to zero, the current density at maximum power,

$$j_c = V_0/2R_{int} \quad (A.3)$$

putting this value of j_c in Eq. (A.2):

$$P_{max} = V_0^2/4R_{int} \quad (A.4)$$

References

[1] B. Johnston, M.C. Mayo, A. Khare, Technovation 25 (2005) 569–585.
[2] B. Rohland, J. Nitsch, H. Wendt, J. Power Sources 37 (1992) 271–277.
[3] N.Q. Minh, Solid State Ionics 174 (2004) 271–277.
[4] N.Q. Minh, J. Am. Ceram. Soc. 76 (1993) 563–588.
[5] V.V. Kharton, F.M.B. Marques, A. Atkinson, Solid State Ionics 174 (2004) 135–149.
[6] V. Jayaraman, A. Magrez, M. Caldes, O. Joubert, M. Ganne, Y. Piffard, L. Brohan, Solid State Ionics 170 (2004) 17–24.
[7] J.B. Goodenough, Solid State Ionics 94 (1997) 17–24.
[8] T. Delahaye, O. Joubert, M.-T. Caldes, Y. Piffard, P. Stevens, Solid State Ionics 177 (2006) 2945–2950.
[9] D. Prakash, R. Ramanathan, B.P. Sharma, Trans. PMAI 29 (2003) 100–104.
[10] C.J. Wen, R. Kato, H. Fukunago, H. Ishitani, K. Yamada, J. Electrochem. Soc. 147 (6) (2000) 2076–2080.
[11] W.Z. Zhu, S.C. Deevi, Mater. Sci. Eng. A362 (2003) 228–239.